Seismic Performance Assessment of a Railway Masonry Arch Bridge Using Sensor-Based Model Updating Approach: A Case Study of Veresk Bridge

Mosabreza Tajali[1]*, Shervan Ataei[1], Amin Miri[2], Ehsan Ahmadi[3], Mohammad M. Kashani[4]

1. School of Railway Engineering, Iran University of Science and Technology, Narmak, Tehran, Iran
2. School of Civil Engineering, Queensland University of Technology, Brisbane, Australia.
3. Faculty of Engineering and the Built Environment, Birmingham City University, Birmingham, UK
4. Faculty of Engineering and Physical Sciences, University of Southampton, UK

**Corresponding author's email: m_tajalli@alumni.iust.ac.ir*

Abstract

A large part of Iranian railway bridge asset comprises masonry arch bridges, which have been in service for over 70 years. Seismic assessment of such structures is of great importance, particularly for high-seismic regions. Hence, this study assesses the seismic performance of Veresk masonry arch bridge, the longest masonry arch bridge of Iranian railway network (a span length of 99 m), spanned over a valley of depth 110 m, through a reliable sensor-based model updating. Dynamic tests are carried out using a test train, composed of 6-axle locomotives and 4-axle freight wagons, which travels across the bridge, and subsequently, vibration response of the instrumented bridge is measured. A high-fidelity 3D Finite Element (FE) model of the bridge is developed and updated using the measured vibration characteristics: mid-span displacements and natural frequencies. Finally, the seismic performance assessment of the bridge is performed through non-linear static and dynamic analyses for two seismic hazard levels with return periods of 150 and 1000 years. It is found that for the hazard level with a return period of 150 years, both nonlinear static and dynamic analyses give very similar results. However, for the seismic hazard level with the return period of 1000 years, the results of the static analysis are more conservative.

Keywords: Seismic Performance Assessment, Masonry Bridge, Field Tests, Model Updating, Finite Element Model.

1. Introduction

Masonry arch bridges are important assets of railway infrastructures, and thus, their health monitoring and seismic performance assessment is an indispensable task. However, some guidelines assess serviceability performance of masonry arch bridges, and their seismic performance is unfortunately ignored (BD 91-04, 2004; UIC 778-3, 2011). Due to lack of knowledge on seismic performance of masonry arch bridges, these guidelines have limited arch bridges to spans of 6 m and 10 m, for areas with high and medium seismicity, respectively (Indian Railway Standard, 2000). Although masonry has small tensile strength, and large bending moments are developed at pier bases of masonry bridges, recent earthquakes exhibit that such structures experience relatively slight damages (UIC 778-3, 2011). These contradictory views of the seismic performance of masonry bridges indicate that a more detailed investigation on their seismic behavior is essential.

There exist a variety of methods for seismic performance assessment of masonry arch bridges. Zampieri et al. (2015) proposed a simplified method to assess failure mechanisms of multi-span arch bridges and grouped them in subclasses with similar modes of failure, based on their geometrical characteristics such as arch length, arch rise, and pier height and width. It was reported that local and global failure mechanisms are likely to occur in longitudinal direction. In transverse direction, however, shear, diagonal cracks, and combined axial-bending failures are among the main mechanisms. Da porto et al. (2016) adopted limit analysis to assess seismic performance of 750 masonry bridges in Italian railway network. The bridges were classified based on their geometrical characteristics and collapse mechanisms. It was found that multi-span bridges with slender piers are the most vulnerable to seismic actions, mostly in transverse direction. Further, single-span bridges with high abutments are highly vulnerable to medium-high seismic forces in longitudinal direction.

Over recent years, non-linear static and dynamic analyses have been performed on 3D FE models as an effective tool for seismic performance assessment of masonry bridges (Ozmen and Sayin, 2018; Zani et al., 2019; Mahmoudi et al., 2018; Yazdani et al., 2019; Bayraktar and Hokelekli, 2021). Non-linear static analysis (NSA) and non-linear dynamic analysis (NDA) have been used to assess seismic performance of masonry structures. Pela et.al (2009) used NSA to assess brick and concrete masonry bridges of three spans. It was concluded that top elevation node is not a suitable controlling point for NSA as the bridge is more deformable at that point, leading to higher safety factors. Additionally, displacement capacity of both bridges was higher than their seismic displacement demand. In a different study, Pela et.al (2013)

performed detailed analysis of a masonry arch bridge to evaluate accuracy of NSA through comparison with NDA. It was seen that displacement response from NSA is slightly higher than mean displacement response from NDAs.

Gonen and Soyoz (2021) showed that updated numerical model of bridges based on experimental results is essential for their seismic performance assessment. An experimental modal analysis using ambient vibration was conducted to characterize material properties of a masonry bridge as well as its global dynamic properties. Aytulun et.al (2022) developed a 3D FE model of a stone arch bridge and evaluated seismic performance of the bridge using NSA and NDA. The FE model was updated based on modal parameters from vibration measurements. It was found that both analysis approaches give similar seismic assessment. In a different study, a historical stone masonry bridge was instrumented by Azzara et al. (2017) using four three-axial seismometric stations. Various operational modal analysis techniques were employed to extract dynamic characteristics of the bridge. They concluded that peak-picking method gives a good estimation of natural frequencies of the bridge; however, covariance-driven stochastic subspace identification method and enhanced frequency domain decomposition method can provide reliable information on the natural frequencies, mode shapes, and damping ratios of the bridge. A 3D FE model of the bridge was also developed and updated, where a relative difference of less than 5% was achieved between the experimental and numerical natural frequencies of the bridge. De Falco et al. (2018) estimated numerical model parameters of the same masonry arch bridge using two different approaches: a deterministic framework and a Bayesian probabilistic method. The former minimizes the difference between the natural frequencies obtained from the experiment and the numerical model, and the latter uses both natural frequencies and mode shapes in a probabilistic framework. It was found that both approaches give very similar frequencies.

As a large part of Iranian railway network bridge asset is composed of masonry arch bridges, this study focuses on seismic performance assessment of an old and historical masonry arch bridge in Iran: Veresk bridge. The bridge is instrumented with various types of sensors first, and then, dynamic tests are performed to measure vibration response of the bridge including acceleration and displacement. The dynamic tests include a test train travelling across the bridge. A 3D FE model of the bridge is developed in ABAQUS software, and validated through sensor-based model updating. The validated FE model is then used to assess seismic performance of the bridge through NSA and NDA approaches for two seismic hazard levels with return periods of 150 and 1000 years.

2. Dynamic Testing and Numerical Modelling of Veresk Bridge

Veresk Bridge is a concrete masonry arch bridge built in 1936 in the northern part of Iran over a valley of height 110 m (Figure 1). It has been registered and recognized as a national heritage site due to its stylish architecture. As shown in Figure 1a, the bridge has a total length of 99 m (the largest span in the Iranian masonry bridge asset). It is composed of a central arch of 66 m, and 8 piers that rest on rock bed and the arch itself. The bridge consists of an approximately 14400 concrete blocks, each with an approximate length of 60 cm, thickness of 25 cm, and varying width of 35 cm to 77 cm. The width of the main arch varies between 4.9 m to 6 m, with a steep gradient of 0.028 %. The thickness of the main arch varies from 2.8 m (at the base) to 1.6 m (in the middle of the span). The bridge is located in Alborz region, which is a highly seismic region in Iran.

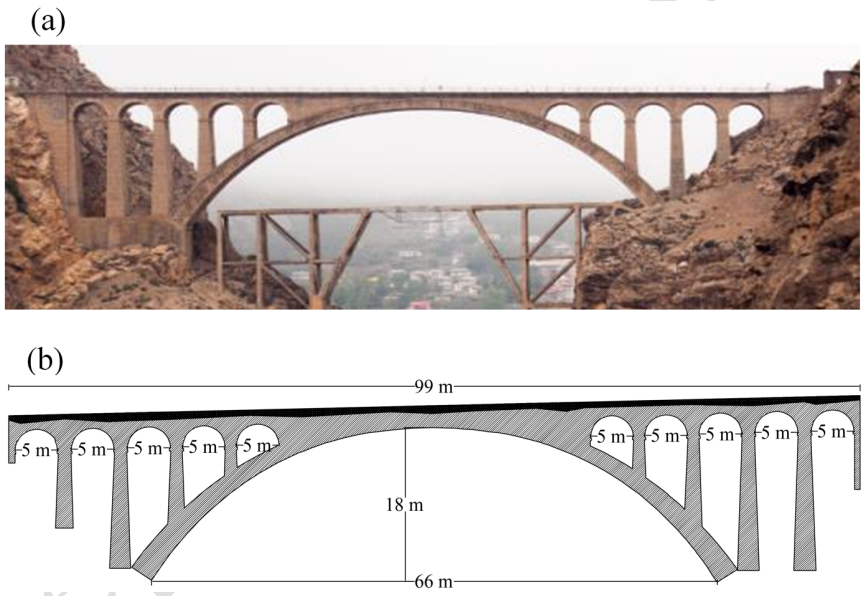

Figure 1. (a) The Veresk Bridge, and (b) its dimensions and geometry.

2.1 Bridge instrumentation and dynamic testing

A thorough seismic assessment of masonry arch bridges require comprehensive information of geometry, foundations and loads, material properties, and load transfer (UIC 778-3, 2011). In reality, however, it is fairly difficult to determine exact material properties of masonry bridges. There are sometimes uncertainties such as boundary conditions and modelling assumptions as well. Therefore, in such cases, field tests are very useful to capture global response of masonry bridges, through applying pre-defined loading scenarios.

In this study, a field test is conducted to determine vibration responses of Veresk Bridge subject to a test train as the loading scenario. The accelerations of the bridge as well as vertical

displacement of the main arch are monitored and measured under travelling of a test train across the bridge. To this end, 5 accelerometers and 2 deflected cantilever displacement transducers (DCDTs) with a frequency of 10 Hz and accuracy of 100 μm are used to collect acceleration and displacement data. Additionally, the rail track is instrumented with linear variable differential transformer (LVDT) sensors and strain gauges to determine the exact speed of the test train and its location on the bridge. Figure 2 shows the bridge dynamic instrumentation including all the sensors. The test train comprises two 6-axle diesel locomotives and two 4-axle freight wagons, as shown in Figure 3. The loading of each axle and their spacing is shown in Figure 3b. The weight of locomotive and the freight wagon were measured by static rail scales at a rail station near to the bridge location.

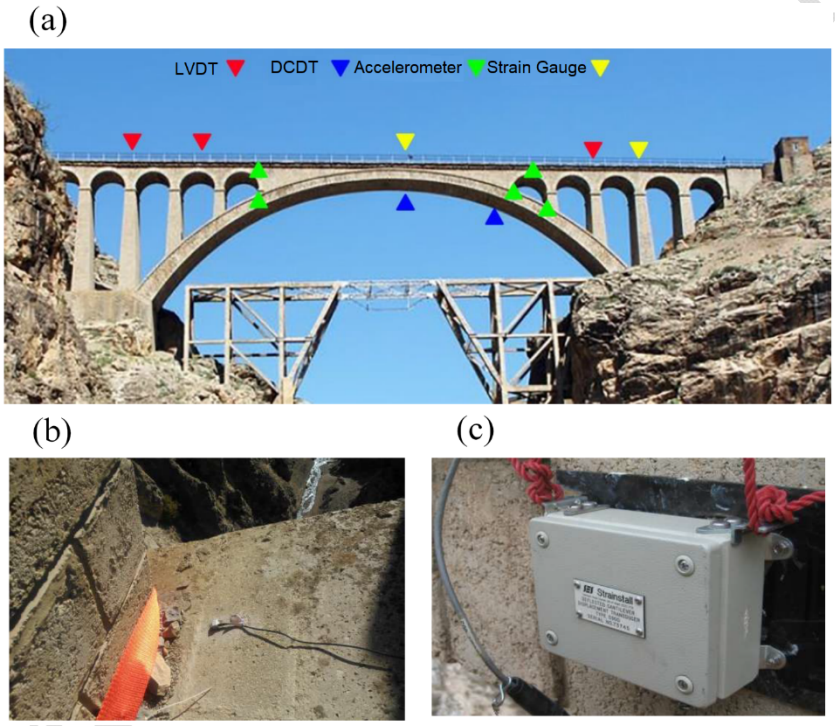

Figure 2. (a) Bridge instrumentation and location of the sensors, (b) accelerometers, and (c) DCDTs.

(a)

(b)

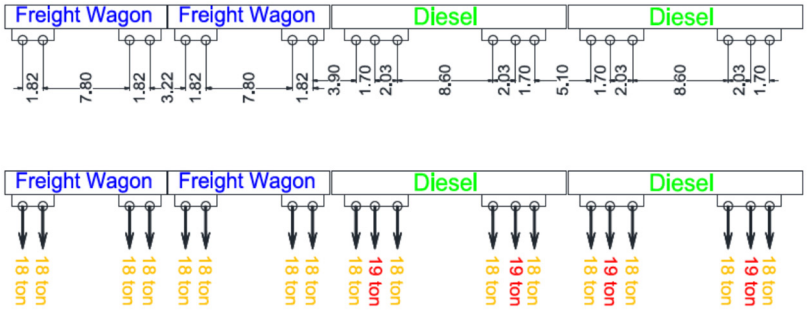

Figure 3. (a) Test train, and (b) axle loads and spacing of the test train.

To have a good estimation of the material properties of the bridge, a series of material tests is conducted. A number of cores from different locations on the bridge are extracted and tested to determine material properties of the concrete bricks. The test results show a mean compressive strength of 28 MPa and an elastic modulus of 25 GPa for the concrete bricks of the arch and piers. There is mortar between the concrete bricks, and hence, equivalent elastic modulus of the masonry unit is calculated to be used in the FE model of the bridge (S.B. 4.7., 2007):

$$E = \frac{E_m E_b \left(t_m + t_b\right)}{E_m t_b + E_b t_m} \tag{1}$$

where E_m and E_b are the elastic modulus of the mortar joint and the concrete brick, respectively; t_m is the thickness of the mortar joint, and t_b is the thickness of the concrete brick. The concrete bricks have a thickness of 25 cm, and the mortar joints have a thickness of 2 cm. According to the construction drawings of the bridge, the mix ratio of the mortar for volume was 1:3 (cement-to-sand), and hence, its elastic modulus was estimated 13.5 GPa based on the test results by Marques et al (2020). Thus, an elastic modulus of 23.5 GPa is calculated for the masonry unit using equation (1). Other material properties, including the density of masonry and Poisson ratio were considered 25 kN/m^3 and 0.2, respectively.

2.2 FE modelling and updating

A 3D FE model of the bridge is developed in ABAQUS software, as shown in Figure 4a. The foundations of the bridge rest on hard lime stone with a mean shear-wave velocity of 2500 m/s (Sadidkhouy and Javan, 2015), and thus, the effects of soil-structure interaction is negligible. So, the restraints of the bridge are modeled as fully-fixed points in the numerical model. The model was developed by 8-node brick elements (C3D8) and a maximum mesh size of 40 cm, which give a total number of 59905 elements and 78275 nodes. The train can be modeled by: (1) a series of moving loads, (2) a series of moving mass, or (3) a series of sprung mass. In this study, the moving load model was employed. Due to the large mass of masonry bridges (i.e. very low train-to-bridge mass ratio), the effect of the train-bridge interaction is negligible, and hence, the moving load model is sufficient for the dynamic analysis of the bridge (Liu et al. 2009).The bridge model is updated to minimize the differences between modal properties and vibration response from the FE model and field testing. This is done by altering material properties and boundary conditions of the model. So, the elastic modulus of the masonry, which has been considered a homogenous medium, is modified to reduce the difference between the simulated and measured vertical displacements at the mid-span of the bridge, as shown in Figure 4b. Then, the updated model is validated through comparing experimental and numerical natural frequencies of the bridge. The free vibration parts of the measured accelerations from the field tests are used to determine the first mode natural frequency of the bridge for various directions, as summarized in Table 1. In this study, peak picking technique, a well-known method of operational modal analysis which uses frequency domain representation of a measured signal, was employed to determine natural frequencies of the bridge. UIC 778-3 mandates that the difference between numerical and experimental natural frequencies of first and second modes shall be less than 15% and 25%, respectively. In this study, the differences between numerical and experimental natural frequencies of the first modes are less than 10%. The updated and verified model is then used to extract the mode shapes of the bridge, as shown in Figure 5. The elastic modulus of the masonry for the verified model is 25 GPa, which is 6% larger than the value predicted by equation (1) (23.5 GPa).

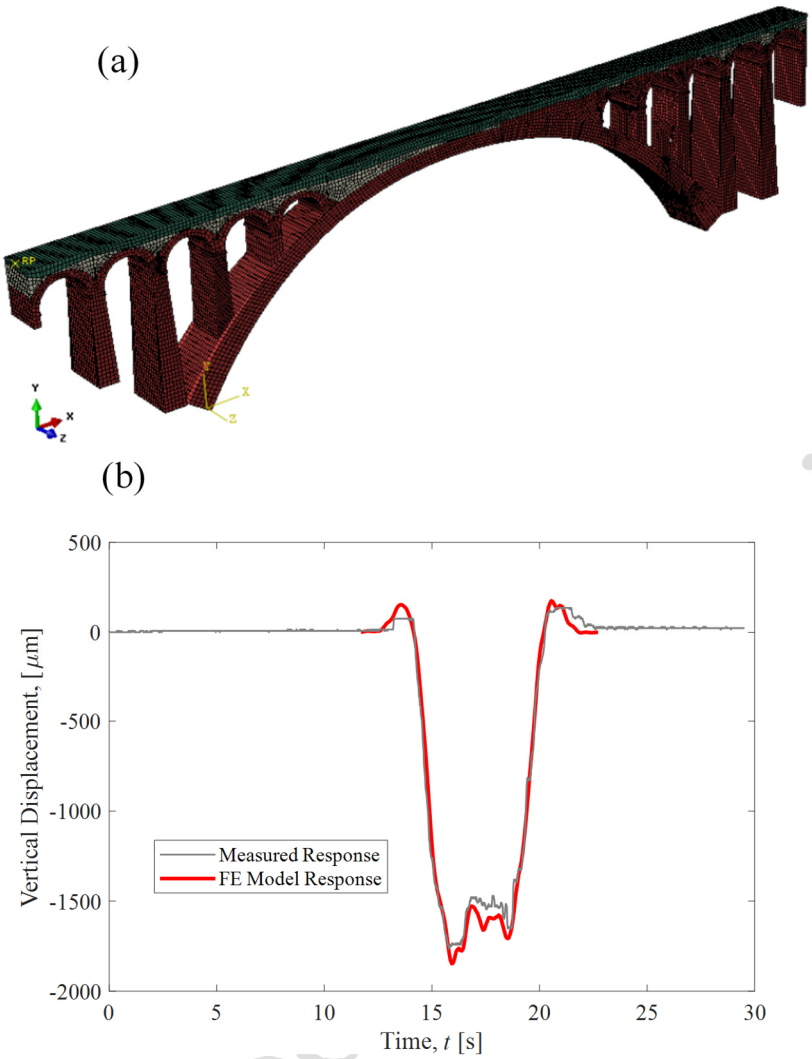

Figure 4. (a) The 3D FE model of Veresk Bridge in ABAQUS, and (b) FE model and measured displacements of the mid-span for the train speed of 50 km/h.

Table 1. Numerical and experimental natural frequencies of the bridge's first mode shape for various directions.

Direction of 1st mode shape	Frequency (Hz)	
	Experimental	Numerical
Transverse	2.1	2.2
Longitudinal	2.9	3.2
Vertical	5.1	5.1

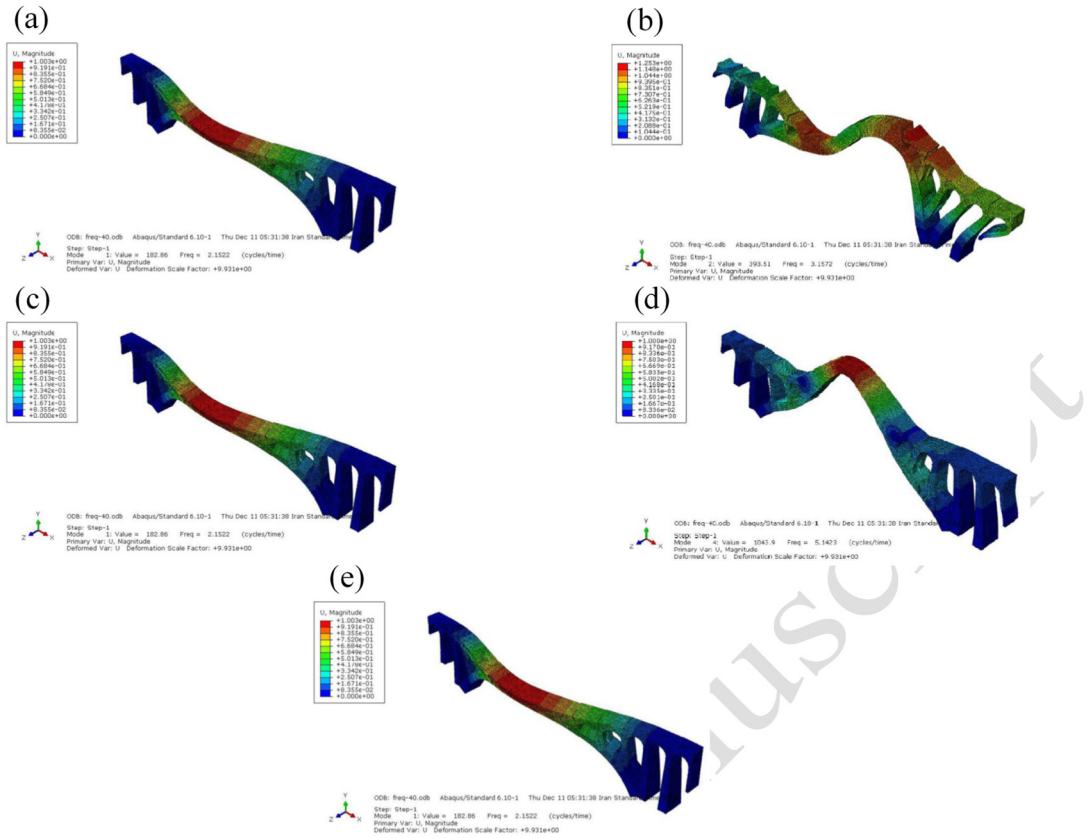

Figure 5. Five vertical mode shapes of Veresk Bridge extracted from the model in ABAQUS: (a) 1st mode shape, (b) 2nd mode shape, (c) 3rd mode shape, (d) 4th mode shape, and (e) 5th mode shape.

To introduce the nonlinearity to the model for seismic analysis of the bridge, a damage plasticity (CDP) model of concrete was chosen (Figure 6). For this model, the compressive strength of the masonry is determined from the equation proposed by Fortes et.al (2015). Thus, the masonry-to-masonry unit compressive ratio and compressive strength of masonry are calculated 0.85 and 23.8 MPa, respectively. The tensile strength of the concrete masonry, σ_{t0}, is $0.63\sigma_{cu}{}^{0.5}$ (MPa), where σ_{cu} is the compressive strength of the concrete masonry, 23.8 MPa (ACI 318-02, 2002). The concrete under compression follows a linear elastic relationship until the value of stress reaches $\sigma_{c0} = 0.45\sigma_{cu}$; afterwards, the hardening behavior is followed by strain softening beyond the compressive strength, σ_{cu}, at the strain, $2\sigma_{cu}/E_0$ (Park and Pauly, 1975). For nonlinear dynamic analysis, Rayleigh damping was used to model the damping of the bridge (Abbasi and Moustafa, 2021). The first two modes of the bridge with damping ratios of 5% was employed based on existing literature on masonry arch bridges (Bayraktar et al. 2015; Moosavi et al. 2016).

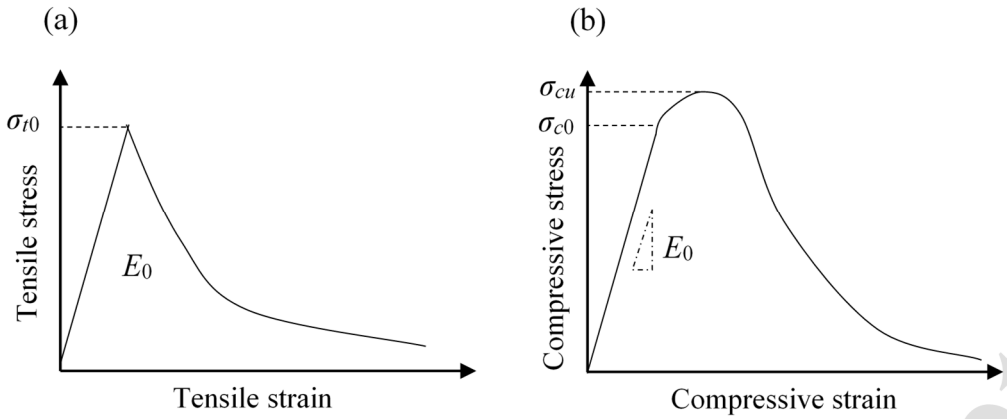

Figure 6. Concrete damage plasticity (CDP) model for: (a) tensile behaviour, and (b) compressive behaviour.

3. Seismic Analyses and Results

3. 1 Nonlinear static analysis

It is common practice to use NSA for seismic analysis of structures. Various NSA methods have been proposed by design codes and guidelines (e.g. Capacity spectrum method in ATC40 (1996), coefficient method in FEMA 356 (2000), and the N2 method in Eurocode 8 (2003) based on the studies of Fajfar (2000; 2002)). In this study, the N2-method is used to assess the seismic performance of Veresk Bridge.

The first step of the N2 method is to determine elastic demand spectrum. Two seismic hazard levels with return periods of 150 years (E1) and 1000 years (E2) are considered, which correspond to serviceability and safety limit states, respectively (see Figure 7a). The elastic demand spectra of E1 and E2 are determined based on probabilistic seismic hazard analysis. As seen in Figure 7a, the both demand spectra have peak values at the period of 0.1 s, which increases with the increase of the return period.

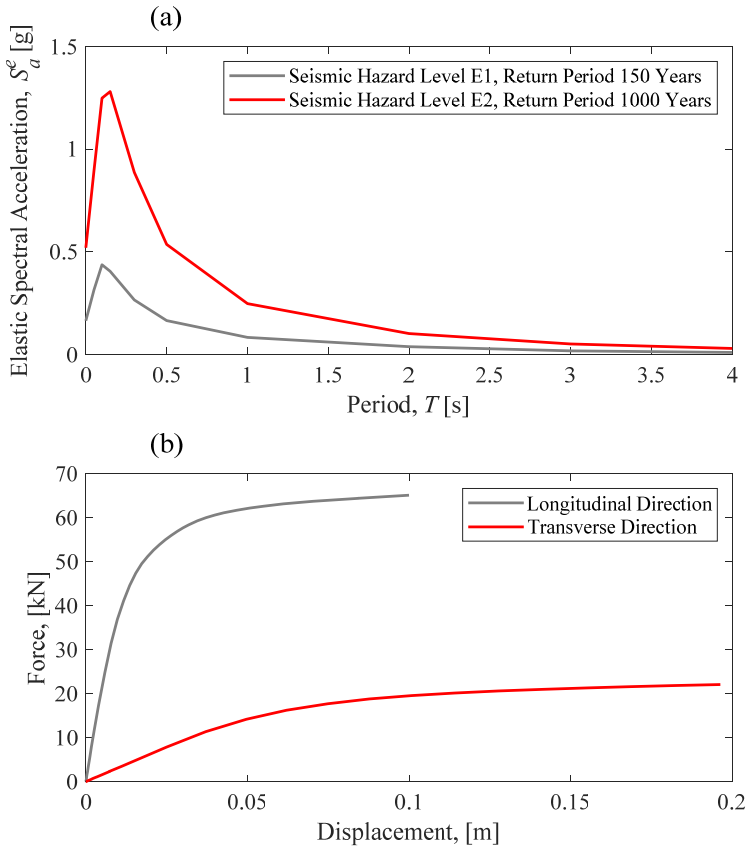

Figure 7. (a) Elastic demand spectrum of the seismic hazard levels, and (b) capacity curves for longitudinal and transverse directions.

To compare the demand spectra with the capacity curves, the demand spectra are presented in an Acceleration-Displacement format (referred to as A-D format). The elastic displacement spectrum is computed from the elastic acceleration spectrum:

$$S_d^e = \frac{T^2}{4\pi^2} S_a^e \tag{2}$$

where S_{ae} and S_{de} are the elastic acceleration and displacement values at a period of T, respectively. The inelastic acceleration and displacement spectra are then determined by Vidic et al. (1994):

$$S_a^{in} = \frac{S_a^e}{R_\mu}; S_d^{in} = \mu \frac{S_d^e}{R_\mu} \tag{3}$$

where μ is the ductility factor defined as the ratio of maximum displacement to yield displacement; R_μ is the strength reduction factor due to ductility, and is given by:

$$R_\mu = \begin{cases} (\mu - 1)\dfrac{T}{T_c} + 1 & T \le T_c \\ \mu & T > T_c \end{cases} \tag{4}$$

in which, T_c is the characteristic period of the ground motion. To determine capacity curves of the bridge (see Figure 7b), lateral loading patterns, compatible with the first mode shapes, are applied to the bridge in transverse and longitudinal directions, and the top node of the bridge is selected as the controlling point (Eurocode 8, (2003)). Afterwards, the capacity curves are approximated with bilinear spectra such that the surface under the approximated curve equals the actual capacity curves. Finally, the maximum inelastic displacement demands are calculated through the intersection of the demand spectra and the capacity curves (see Figure 8).

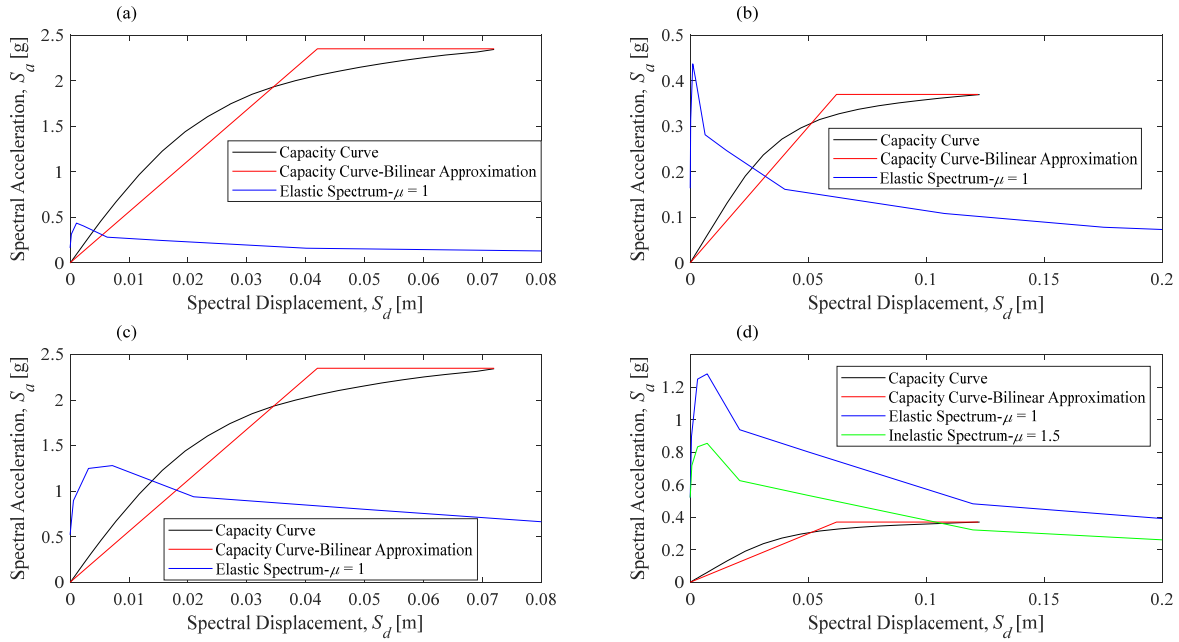

Figure 8. Capacity curves and demand spectra for: (a) E1 and longitudinal direction, (b) E1 and transverse direction, (c) E2 and longitudinal direction, and (d) E2 and transverse direction.

As seen in Figure 8, the ductility factor, μ, of the bridge is 1.5 for E2 earthquake in transverse direction, while it is 1.0 for other cases. Given the fundamental periods of the bridge in longitudinal and transverse directions, respectively 0.34 s and 0.48 s, and characteristic period of the ground motion, T_c = 0.4 s, the reduction factors, R_μ, are determined using equation (4). Table 2 summarizes the results of the ductility and reduction factors.

Table 2: Ductility and reduction factors of the bridge.

Earthquake characteristics		Ductility factor (μ)	reduction factor (R_μ)
Direction	Return Period (year)		
Longitudinal	150	1.0	1.0
	1000	1.0	1.0
Transverse	150	1.0	1.0
	1000	1.5	1.5

Damage modes for longitudinal and lateral loadings are shown in Figure 9. As seen in Figure 9a, for tensile damages due to the longitudinal earthquake, four-hinge mechanism of the main arch are formed. Further, plastic hinges are developed at the base of some piers located on and at the end of the main arch. Some plastic hinges are also created at the top node of some piers, which result in mechanism failure of the piers. Mechanism failure also occurs for the lateral earthquake, as three hinges (two at the bottom nodes of the columns and one in the middle of the arch) are formed in the main arch of the bridge. Plastic hinges are also seen in some of the smaller spans. The maximum displacement for the longitudinal and transverse directions are respectively 10.1 cm and 19.6 cm. The longitudinal and transverse deformability of the bridge (maximum-to-yield displacement ratios) are 1.71 and 1.97, respectively.

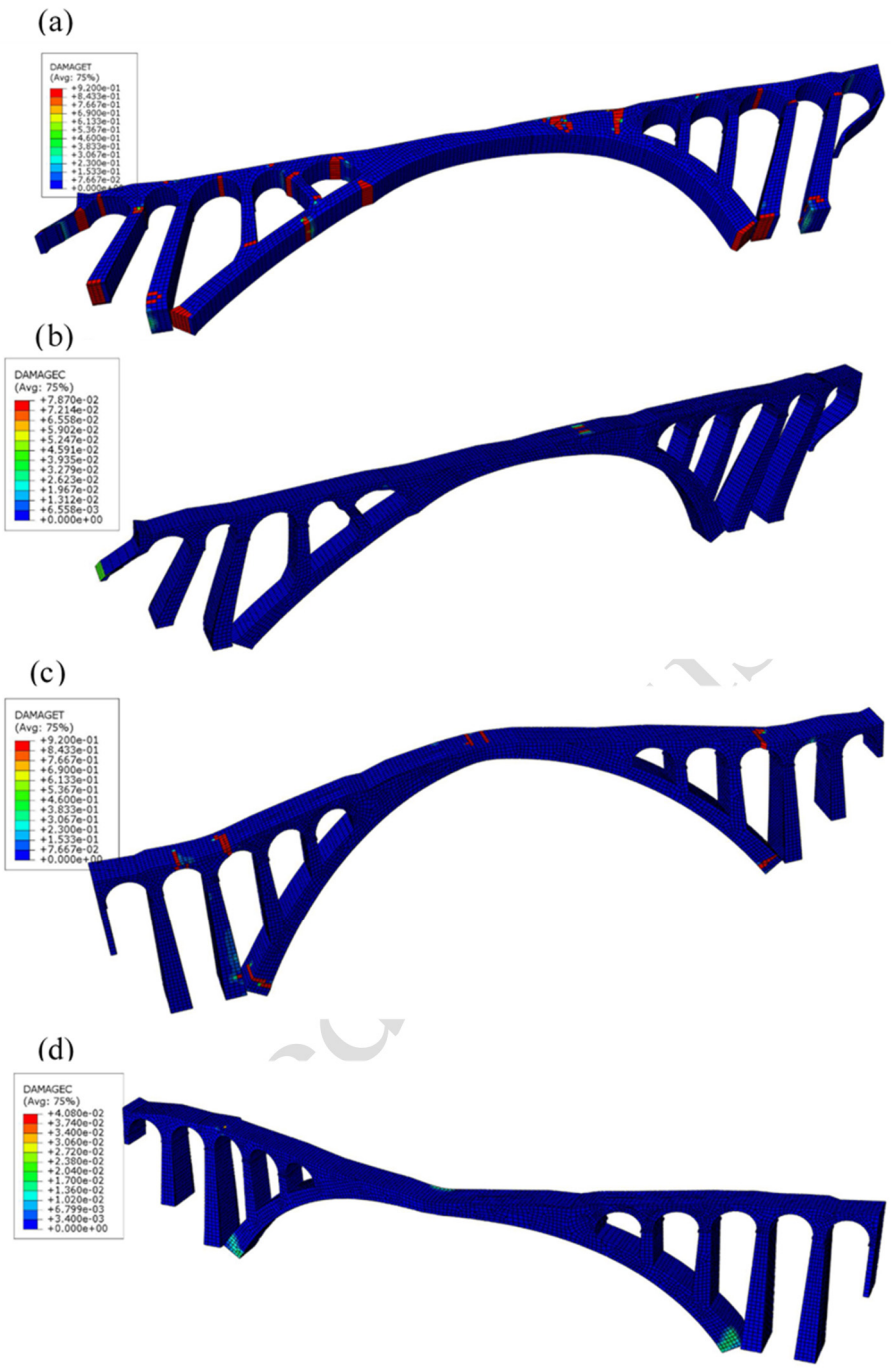

Figure 9. Developed damage modes at the maximum inelastic displacements: (a) tensile damage for longitudinal earthquake, (b) compressive damage for longitudinal earthquake, (c) tensile damage for transverse earthquake, and (d) compressive damage for transverse earthquake.

3. 2 Nonlinear dynamic analysis

To perform NDA, Euro-Code 8 recommends at least three pairs of horizontal acceleration ground motion records. Thus, three horizontal ground motion records from Manjil, Kobe and Hector earthquakes are selected, and scaled for seismic hazard levels E1 and E2 prior to being used in NDA. To scale each record, the square root of the sum of the squares (SRSS) elastic

spectrum is determined for damping of 5% (Figure 10a), and then, the mean-spectrum is generated across the three records (Figure 10b). Afterwards, the SRSS spectrum for each record is scaled so that the mean-scaled spectrum is not lower than 1.3 times the 5% damped elastic spectrum of the seismic hazard level, over the period range between $0.2T_b$ and $1.5T_b$, where T_b is the period of the fundamental mode of the bridge (Figures 10b).

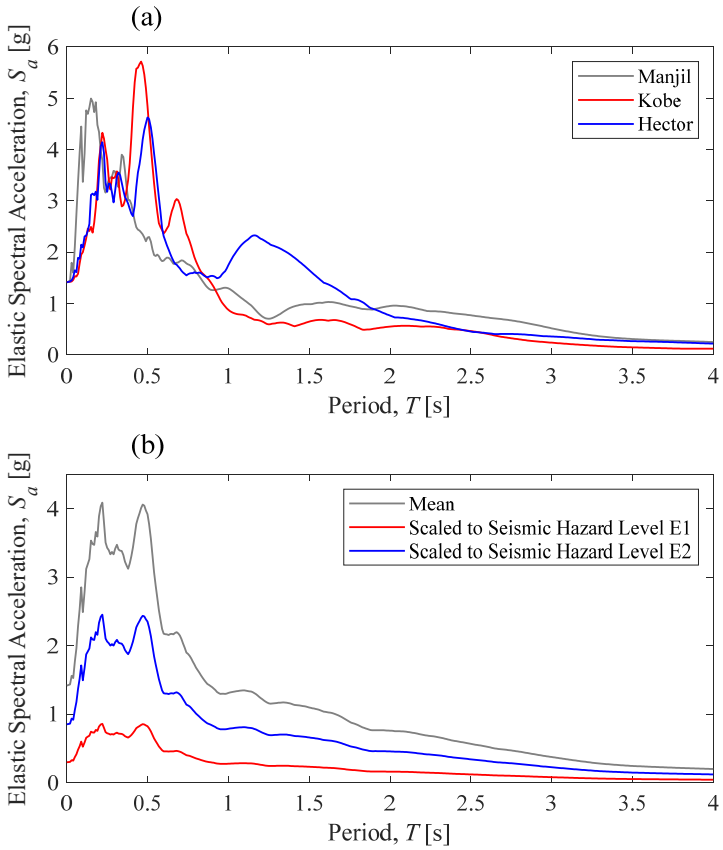

Figure 10. (a) Elastic spectra of the three horizontal records, and (b) mean and scaled spectra.

Figure 11 shows the displacement time history of the bridge for various seismic hazard levels and directions. As seen, residual displacements are significantly higher for seismic hazard level E2 compared to E1. Table 2 compares maximum displacement of the bridge for various analyses, seismic hazard levels and directions. As seen in Table 2, for seismic hazard level E1 (serviceability state), the maximum displacement of the bridge from both NSA and NDA are similar. For seismic hazard level E2 (safety state), however, NSA gives rather conservative values. According to FEMA 356, permissible drift of masonry structures in rocking mode, which is the most common mode of failure of masonry bridges in transverse direction, for immediate occupancy, life safety, and collapse prevention performance levels are 0.1%, 0.96%, and 1.29%, respectively. For Veresk Bridge, displacement values of 1.8 cm, 17.3 cm, and 23.2 cm are computed for performance levels of immediate occupancy, life safety, and collapse

prevention. However, the maximum displacements resulting from safety level earthquake E2 (Table 3) are lower than the permissible displacement of the bridge for life safety, 17.3 cm, and the immediate occupancy performance level is not satisfied for serviceability earthquake E1.

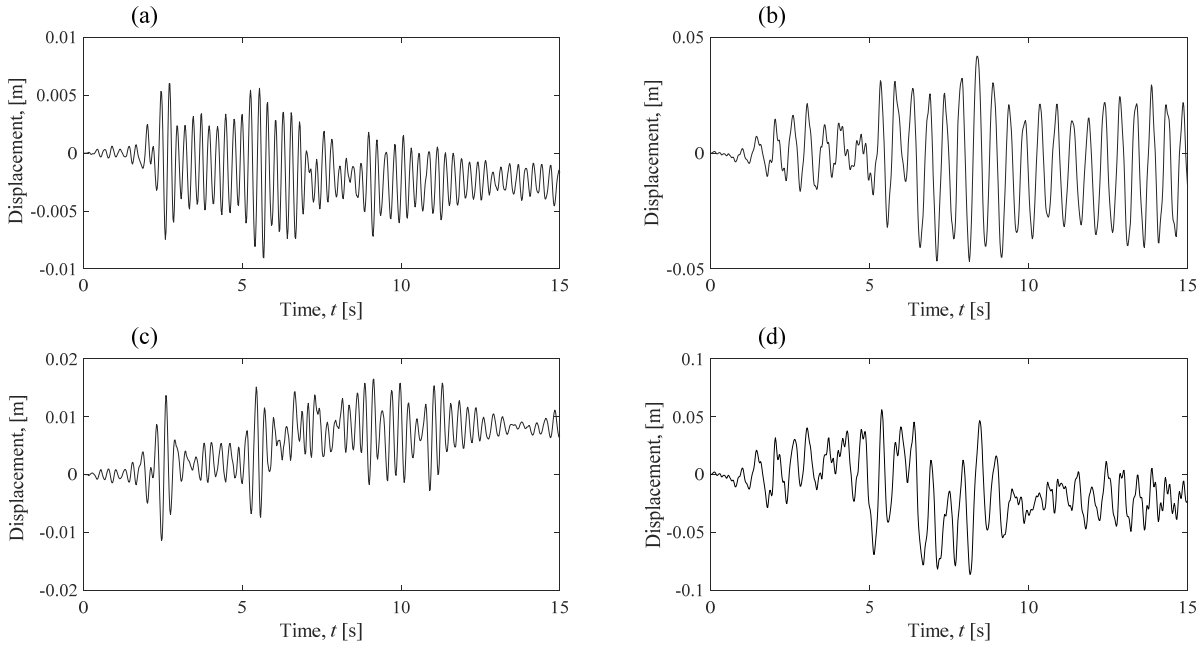

Figure 10. Bridge displacement response for Manjil earthquake for: (a) seismic hazard level E1 and longitudinal direction, (b) seismic hazard level E1 and transverse direction, (c) seismic hazard level E2 and longitudinal direction, and (d) seismic hazard level E2 and transverse direction.

Table 3: Maximum displacement of Veresk Bridge from NSA and NDA for longitudinal and transverse directions.

Earthquake characteristics		Maximum displacement of the bridge (cm)	
Direction	Return Period (year)	NSA	NDA
Longitudinal	150	0.77	0.89
	1000	2.8	2.11
Transverse	150	4.96	5.01
	1000	15.2	9.98

4. Conclusion

Seismic performance assessment of Veresk Bridge, an old masonry ach bridge, is presented through a sensor-based model updating approach. In-situ material tests and dynamic tests were performed for the bridge. The results of the dynamic tests were used to update and verify the 3D FE model of the bridge developed in ABAQUS. Finally, nonlinear static and dynamic analyses were performed to assess seismic performance of Veresk Bridge.

It was found from the non-linear static analyses that, four plastic hinges are formed in the main arch of the bridge, which result in failure mechanism of the arch in longitudinal direction. Failure mechanism also occurs in some piers with plastic hinges at the top and bottom. In

transverse direction, three hinges are developed in the main arch of the bridge. Deformability factors of the bridge in longitudinal and transverse directions are 1.71 and 1.97, respectively. For the non-linear dynamic analyses, two seismic hazard levels were used: return periods of 150 years (serviceability level) and 1000 years (safety level). It is seen that for the serviceability level, two methods produce almost identical results, while for the safety level, non-linear dynamic analyses are more conservative. Further, life safety performance level is achieved for both seismic hazard levels.

References

Abbasi M., Moustafa M.A., (2021), 'Effect of Damping Modeling and Characteristics on Seismic Vulnerability Assessment of Multi-Frame Bridges', Journal of Earthquake Engineering, Vol. 25(8), 1616-43.

ACI 318-02, (2002), 'Building code requirements for structural concrete', American Concrete Institute.

ATC 40, (1996), 'Seismic evaluation and retrofit of concrete buildings', Redwood city: Applied technology council.

Aytulun E, Soyoz S and Karcioglu E., (2022), 'System Identification and Seismic Performance Assessment of a Stone Arch Bridge', Journal of Earthquake Engineering, Vol. 26(2), 723-743.

Azzara M., De Falco A., Girardi M. and Pellegrini D., (2017), 'Ambient vibration recording on the Maddalena Bridge in Borgo a Mozzano (Italy): data analysis', Annals of Geophysics, Vol. 60(4), S0441.

Bayraktar A., and Hökelekli E., (2021), 'Seismic Performances of Different Spandrel Wall Strengthening Techniques in Masonry Arch Bridges, International Journal of Architectural Heritage, Vol. 15(11), 1722-1740,

Bayraktar A., Türker T., Altunişik A., (2015), 'Experimental frequencies and damping ratios for historical masonry arch bridges', Construction and Building Materials, Vol. 75, 234-241.

Code BD 91/04, (2004), 'Design Manual for Roads and Bridges', Unreinforced masonry arch bridges.

Da Porto F., Tecchio G., Zampierei P., Modena C., and Prota A., (2016), 'Simplified seismic assessment of railway masonry arch bridges by limit analysis', Structure and Infrastructure Engineering, Vol.12(5).

De Falco A., Girardi M., Pellegrini D., Robol L., and Sevieri G., (2018), 'Model parameter estimation using Bayesian and deterministic approaches: the case study of the Maddalena Bridge', Periodica Structural Integrity, Vol.11, 210-217.

Eurocode 8, (2003), 'Design of structures for earthquake resistance, Part 1: General rules, seismic actions and rules for buildings'.

Fajfar, P., (2000), ‘A nonlinear analysis method for performance-based seismic design’, Earthquake Spectra, Vol. 16(3), 573-592.

Fajfar, P. (2002), ‘Structural analysis in earthquake engineering, a breakthrough of simplified nonlinear methods’, 12th European Conference on Earthquake Engineering.

FEMA 356, (2000), ‘Pre-standard and commentary for the seismic rehabilitation of buildings’, Washington (DC): Federal Emergency Management Agency.

Fortes E., Parsekian G., and Fonseca F., (2015), 'Relationship between the compressive strength of concrete masonry and the compressive strength of concrete masonry units', Journal of Material in Civil Engineering, Vol. 27(9).

Gönen S and Soyöz z, (2021), ‘Seismic analysis of a masonry arch bridge using multiple methodologies’, Engineering Structures, Vol. 226-111354.

Indian Railway Standard, (2000), ‘Code of practice for the design and construction of masonry and plain concrete arch bridge’.

Liu K., De Roeck G., and Lombaert G., (2009), ‘The effect of dynamic train–bridge interaction on the bridge response during a train passage’, Journal of Sound and Vibration, Vol.325, 240-251.

Mahmoudi M., Hasani N., and Yazdani M., (2018), ‘Three-dimensional modelling for seismic assessment of plain concrete arch bridges’, Proceedings of the Institution of Civil Engineers - Civil Engineering, Vol. 171(3), 135-143.

Marques A., Morais J., Morais P., Veiga M., Santos C., Candeias P. and Ferreira G., (2020), ‘ Modulus of elasticity of mortars: Static and dynamic analyses’, Construction and Building Materials, Vol. 232, 117216.

Moosavi M., Ziyaeifar M., Nekooei M., Mokari J., (2016), ‘Effects of vertical motions on seismic response of Goltzschtal masonry arch bridge’, JSEE, Vol. 18(1), 33-46.

Ozmen A. and Sayin E., (2018), ‘Seismic assessment of a historical masonry arch bridge’, Journal of Structural Engineering & Applied Mechanics, Vol. 1(2), 95-104.

Park R., and Pauly T., (1975), 'Reinforced concrete structures', John Wiley and Sons.

Pela L., Aprile A., and Benedetti A., (2009), ‘Seismic assessment of masonry arch bridges’, Engineering Structures, Vol. 31, 1777-1788.

Pela L., Aprile A., and Benedetti A., (2013), ‘Comparison of seismic assessment procedures for masonry arch bridges’, Construction and Building Material, Vol. 38, 381–394

Sadidkhouy, and Javan, (2015), ‘Veresk’s Seismic analyses report’, Iran University of Science and Technology (in Persian).

SB 4.7, (2007), 'Structural assessment of masonry arch bridges', Prepared by 'Sustainable bridges.net'.

UIC 778-3, 2nd Edition, (2011), ‘Recommendations for the inspection, assessment and maintenance of masonry arch bridges’.

Vidic T, Fajfar P, and Fischinger M., (1994), ‘Consistent inelastic design spectra: Strength and displacement’, Earthquake Engineering and Structural Dynamics, Vol. 23, 502–521.

Yazdani M., Jahangiri V. and Marefat MS., (2019), 'Seismic performance assessment of plain concrete arch bridges under near-field earthquakes using incremental dynamic analysis'. Engineering Failure Analysis, Vol 106, 104170.

Zampieri P., Zanini M., and Modena C., (2015), 'Simplified seismic assessment of multi-span masonry arch bridges', Bulletin of Earthquake Engineering, Vol. 13, 2629-2646.

Zani G., Martinelli P., Galli A., Gentile C. and Prisco M., (2019), 'Seismic assessment of a 14th-century stone arch bridge: role of soil-structure interaction', Journal of Bridge Engineering, Vol. 24(7).